Simulation of CO_2 / H_2S Using Thermodynamic and Electrochemical Models

Andrzej Anderko and Robert D. Young

OLI Systems Inc.
108 American Road, Morris Plains, NJ 07950, USA

January, 1999

Simulation of CO_2 / H_2S Corrosion Using Thermodynamic And Electrochemical Models

Andrzej Anderko and Robert D. Young

OLI Systems Inc.,
108 American Road, Morris Plains, NJ 07950

Abstract

A comprehensive model has been developed for the computation of corrosion rates of carbon steels in the presence of carbon dioxide, hydrogen sulfide and aqueous brines. The model combines a thermodynamic model that provides realistic speciation of aqueous systems with an electrochemical model for partial cathodic and anodic processes on the metal surface. The partial processes taken into account by the model include the oxidation of iron and reduction of hydrogen ions, water, carbonic acid and hydrogen sulfide. Also, the model includes the formation of iron carbonate and iron sulfide scales and their effect on the rate of general corrosion as a function of temperature and solution chemistry. The model has been verified by comparing calculated corrosion rates with laboratory data under conditions that may or may not be conducive to the formation of protective scales. Good agreement between the calculated and experimental corrosion rates has been obtained. The model has been incorporated into a program that makes it possible to analyze the effects of various conditions such as temperature, pressure, solution composition or flow velocity on corrosion rates.

KEY WORDS: CO_2 corrosion, H_2S corrosion, iron carbonate, iron sulfide, electrochemical model, thermodynamics

Introduction

Corrosion by carbon dioxide with or without the presence of hydrogen sulfide is an important issue in the oil and gas industry. The severity of corrosion depends on multiple factors including temperature, pressure, pH, composition of the aqueous stream, partial pressures of CO_2 and H_2S, presence of nonaqueous phases, flow conditions and metal characteristics. Therefore, there is a need for models that would predict corrosion rates under various conditions and, thus, save the cost of performing numerous experiments. In view of the multitude of independent variables, the model should lend itself to extrapolation with respect to each major factor that influences corrosion rates. It can be expected that this can be achieved by a mechanistic model that realistically addresses the most important processes on the surface of corroding metals.

Models for CO_2 corrosion have been developed by several investigators[1-16] in the form of semi-empirical correlations, expert systems or electrochemical models for surface reactions. A particular challenge for model development has been the effect of iron carbonate scales.[16] In the case of H_2S corrosion, experimental studies have been performed by various authors.[17-24] These studies included the effect of H_2S on cathodic and anodic processes and the formation of various crystalline forms of iron sulfide scales. However, no predictive mechanistic models have been published in the open literature for H_2S or CO_2/H_2S corrosion.

Therefore, there is a need for developing a model that would simulate corrosion in systems that contain both H_2S and CO_2. Additionally, it is desirable to include the full chemistry of aqueous media that are encountered in industrial practice. For this purpose, it is evident that the model should include both thermophysical and electrochemical modules. The thermophysical module should predict the full speciation, activities of all species and phase equilibria in the system. Additionally, the module should include the transport properties (i.e., diffusivity and viscosity) that are necessary for the computation of flow effects on corrosion. The electrochemical module should predict the surface processes that lead to corrosion as a function of solution chemistry, flow conditions and metal characteristics.

Thus, the objective of this work is to develop a model that

(1) Utilizes a comprehensive thermodynamic model to compute the activities of species that participate in corrosion processes;

(2) Includes the partial cathodic and anodic processes that are responsible for CO_2 corrosion according to the mechanisms determined in the literature;

(3) Proposes additional partial processes that explain the effects of H_2S;

(4) Includes the effects of iron carbonate and iron sulfide scales on corrosion rates and

(5) Reproduces observed corrosion rates using a reasonable set of physically meaningful parameters.

Thermophysical Module

The starting point for corrosion analysis is the computation of speciation in the investigated system. For this purpose, a realistic model of electrolyte systems is used. This model combines information about standard-state properties of all species of interest with a formulation for the excess Gibbs energy, which accounts for solution nonideality. The model has been described in detail by Zemaitis et al.[25] and Rafal et al.[26] In previous studies, the model has been extensively validated against experimental data[25,26] and applied to investigate the stability of various products of H_2S corrosion.[27] Here, the essential elements of the model are summarized in Appendix A.

The thermodynamic model is used to predict the concentrations and activities of both ionic and molecular species in multicomponent systems that may contain an aqueous phase, any number of solid phases and, if necessary, a vapor and a nonaqueous liquid phase. The activities of individual species are further used in the electrochemical model. After completing speciation calculations, the module computes the viscosity of the solution and diffusivities of all species using previously developed models.[36,39]

Electrochemical Model

The electrochemical model takes into account reactions on the surface of the metal and transport processes for the species that participate in the reactions. The model focuses on partial cathodic and anodic processes that are expected to be important in systems containing carbon dioxide and hydrogen sulfide. Further, the model combines the partial processes to compute corrosion rates in the framework of the mixed potential theory.

Anodic Reactions

The mechanism of anodic dissolution of iron has been extensively investigated in acidic solutions (cf. a review by Drazic[28]). While several variations of the mechanism have been proposed, the dependence of the dissolution rate on the activity of hydroxide ions is generally accepted. The mechanism proposed by Bockris et al.[29], i.e.,

$$Fe + OH^- \rightarrow FeOH + e^- \quad (1)$$
$$FeOH \rightarrow FeOH^+ + e^- \ (RD) \quad (2)$$
$$FeOH^+ \rightarrow Fe^{2+} + OH^- \quad (3)$$

predicts that the reaction order with respect to the OH^- ion is 1. The validity of this prediction has been verified for acidic solutions[30]. Additionally, the current density for iron dissolution has been found to depend on the activity of water[31]. The mechanism of Bockris et al.[29] also predicts that the anodic transfer coefficient is equal to 1.5, which gives the Tafel slope of 40 mV at room temperature. Thus, the current density for Fe dissolution is given by

$$i_{Fe} = i_{Fe}^0 \exp\left[\frac{a_{Fe} F\left(E - E_{Fe}^0\right)}{RT}\right] \quad (4)$$

where i_{Fe}^0 is the exchange current density, a_{Fe} = 1.5 and E^0 is the reversible potential of Fe dissolution. The exchange current density can be expressed as

$$i_{Fe}^0 = i_{Fe}^* a_{OH} a_{H_2O}^c \quad (5)$$

where c is a reaction order with respect to the activity of water. According to Smart and Bockris[31], c = 1.6. The effect of the activity of water on the current density is significant only for concentrated solutions, for which the activity of water may differ significantly from one.

Although the reaction order with respect to OH^- ions is valid for acidic solutions, it has been found that iron dissolution proceeds with little influence of pH for solutions with pH above approximately 4.[29] In particular, the lack of a pH effect has been found for CO_2 corrosion (cf., Nesic et al.[12]). Bockris et al.[29] explained this phenomenon by assuming a certain nonzero reaction order with respect to Fe^{2+} and considering the hydrolysis of the Fe^{2+} ions that result from the dissolution. Alternatively, the change in the reaction order with respect to OH^- ions can be reproduced by assuming that the exchange current density is proportional to the surface coverage by OH^- ions. This assumption is consistent with the reaction mechanism (cf. eq. 1). Thus, eq. (5) can be modified as

$$i_{Fe}^{0} = i_{Fe}^{*} q_{OH} a_{H_2O}^{c} \quad (6)$$

Assuming that q_{OH} follows the Langmuir adsorption model, eq. (6) can be rewritten as

$$i_{Fe}^{0} = i_{Fe}^{*} \frac{a_{OH}}{1 + K_{OH} a_{OH}} a_{H_2O}^{c} \quad (7)$$

It should be noted that eq. (7) reduces to eq. (5) for low activities of OH^-, i.e., for acidic solutions. For higher concentrations, the reaction order with respect to OH^- becomes zero. This behavior is illustrated in Figure 1 for pure Fe. A good agreement with experimental exchange current densities[29] has been obtained.

The reversible potential is calculated from the Nernst equation[32] and depends on the activity of Fe^{2+} ions. As shown by West[33] and Nesic et al.[12], a relationship exists between the reversible potential and the exchange current density, i.e.,

$$\frac{RT}{a_{Fe} F} \ln \frac{i_{Fe}^{0}}{i_{Fe}^{0}{}'} = E_{Fe}^{0} - E_{Fe}^{0}{}' \quad (8)$$

Eq. (8) makes it possible to compute the exchange current density for any concentration of ferrous ions once it is established for any reference concentration of Fe^{2+}. The final expression for the anodic current density is a combination of eqs. (4), (7) and (8).

Cathodic Reactions for CO_2 Corrosion

In CO_2 corrosion, cathodic processes may be due to the reduction of four separate species, i.e., H^+, H_2O, H_2CO_3 and HCO_3^- .[34,1,12,16] In acidic solutions, the reduction of H^+ is the dominant cathodic reaction:

$$H^+ + e^- \rightarrow 0.5\ H_2 \quad (9)$$

It is generally accepted that the H^+ reduction reaction may proceed under activation or mass transfer control[32]. According to basic electrochemical kinetics[32], the current density for H^+ reduction can be written as

$$\frac{1}{i_H} = \frac{1}{i_{H,a}} + \frac{1}{i_{H,\lim}} \quad (10)$$

where $i_{H,a}$ and $i_{H,\lim}$ are the activation and limiting current densities, respectively. The activation current density for proton reduction is

$$i_{H,a} = i_H^0 \exp\left[\frac{-a_H F\left(E - E_H^0\right)}{RT}\right] \quad (11)$$

where $\alpha_H = 0.5$[29] and E_H^0 is calculated from the Nernst equation using the previously calculated activities of hydrogen ions and elemental hydrogen. The exchange current density is given by

$$i_H^0 = i_H^* a_H^{0.5} a_{H_2O}^{2.2} \tag{12}$$

In eq. (12), the reaction orders with respect to the activities of H^+ and H_2O have been obtained from the studies of Bockris et al.[29] and Smart and Bockris[31].

The limiting current density in eq. (10) results from diffusion-limited transport of protons to the metal surface and can be calculated as

$$i_{H,\lim} = k_m F a_H \tag{13}$$

where k_m is the mass transfer coefficient. The value of k_m can be calculated if the flow regime, diffusion coefficient of H^+ ions and solution viscosity are known. The formulas for the computation of k_m are collected in Appendix B.

In addition to the reduction of H^+ ions, the direct reduction of water is also considered, i.e.,

$$H_2O + e^- \rightarrow 0.5H_2 + OH^- \tag{14}$$

Unlike the reduction of protons, the water reduction does not exhibit a limiting current density because there are no diffusion limitations for the transport of H_2O molecules to the surface. Thus, the current density can be expressed as:

$$i_{H_2O} = i_{H_2O}^0 \exp\left[\frac{-a_{H_2O} F\left(E - E_H^0\right)}{RT}\right] \tag{15}$$

As for proton reduction, $\alpha_{H2O} = 0.5$. The reversible potential in eq. (15) is the same as in eq. (11) because the reduction of water is thermodynamically equivalent to the reduction of protons. It is reasonable to assume that the reaction order with respect to water activity is the same as that for proton reduction. Thus, the exchange current density is given by

$$i_{H_2O}^0 = i_{H_2O}^* a_H^{-0.5} a_{H_2O}^{2.2} \tag{16}$$

At mildly acidic conditions (pH > 4), reduction of carbonic acid (H_2CO_3) becomes the dominant cathodic process. Carbonic acid results from the hydration of dissolved CO_2, i.e.,

$$CO_2 + H_2O = H_2CO_3 \tag{17}$$

Reaction (17) is followed by the reduction of H_2CO_3 on the surface[1], i.e.,

$$H_2CO_3 + e^- \rightarrow 0.5H_2 + OH^- \tag{18}$$

The H_2CO_3 reduction is under activation or chemical reaction control, i.e.,

$$\frac{1}{i_{H_2CO_3}} = \frac{1}{i_{H_2CO_3,a}} + \frac{1}{i_{H_2CO_3,\lim}} \tag{19}$$

The activation current is given by

$$i_{H_2CO_3} = i^0_{H_2CO_3} \exp\left[\frac{-a_{H_2CO_3} F\left(E - E^0_H\right)}{RT}\right] \tag{20}$$

where the transfer coefficient can be assumed equal to that for H_2O reduction. Also, the reversible potential is equal to that for H^+ or H_2O reduction. The exchange current density for H_2CO_3 reduction can be expressed as:[12]

$$i^0_{H_2CO_3} = i^*_{H_2CO_3} a_{H_2CO_3} a_H^{-0.5} \tag{21}$$

Following Nesic et al.[12], the limiting current density can be expressed using an equation originally derived by Vetter[32] for processes with a rate-determining reaction in the solution. Here, the rate-determining reaction is the hydration of CO_2 and the limiting current density is

$$i_{H_2CO_3,\lim} = Fa_{H_2CO_3} (D_{H_2CO_3} K_{H_2CO_3} k^f_{H_2CO_3})^{1/2} \tag{22}$$

where D_{H2CO3}, K_{H2CO3} and k^f_{H2CO3} are the diffusion coefficient of H_2CO_3, equilibrium constant for the hydration of CO_2 and forward reaction for the hydration reaction, respectively. D_{H2CO3} is calculated from the model of Anderko and Lencka[36], K_{H2CO3} is obtained from the thermodynamic model (Appendix A) and k^f_{H2CO3} is calculated from the temperature-dependent expression developed by Nesic et al.[12]

Another possible cathodic reaction in CO_2-containing systems is the reduction of HCO_3^- ions. However, this reaction is expected to become important for more alkaline solutions than those considered in this study and, therefore, does not have to be analyzed here.

For all partial processes, the concentration-independent part of the exchange current density (i.e., i^*) is assumed to be temperature dependent by introducing a non-zero enthalpy of activation, i.e.,

$$i^*(T) = i^*(T_{ref}) \exp\left[-\frac{\Delta H}{R}\left(\frac{1}{T} - \frac{1}{T_{ref}}\right)\right] \tag{23}$$

Scale Formation

Corrosion processes become significantly more complex in the presence of solid scales that may form on the metal surface. In general, it is necessary to consider (1) the precipitation equilibria on the metal surface; (2) anodic dissolution processes that occur on the free surface of the metal; (3) dissolution

kinetics of the solid scale; (4) cathodic processes on the free metal surface; (5) cathodic processes on the scale surface, which are expected to be considerably slower than those on the free surface; (6) local concentrations of active ions close to the metal surface, which are influenced by adsorption and mass transfer and are usually different from those in the bulk and (7) transport of ions through the scale, which depends on the permeability of the solid precipitate.

In principle, it is possible to develop a truly comprehensive model that takes into account all of these phenomena. However, such a model would contain a very large number of parameters that could not be unequivocally determined on the basis of the limited amount of electrochemical and exposure data that are available in the literature. Therefore, some simplifications are necessary. For this purpose, we introduce an average fraction of the metal surface that is covered by the scale. Further, we assume that the anodic and cathodic processes occur only on the fraction of the surface that is not covered by the scale. This is equivalent to assuming that the scale coverage fraction represents only a protective scale and does not include nonprotective scales. With this simplifying assumption, it is not necessary to treat explicitly the permeability of the solid precipitate. Further, the model recognizes the local concentrations of active species in two ways. For mass transfer-limited processes such as proton reduction on the metal surface, eq. (10) is used, which was derived by considering the differences between local and bulk concentrations due to mass transfer limitations. A similar equation is valid for the transport of ferrous ions away from the scale-covered surface. For other species (such as the CO_2-bearing species that are responsible for scale formation), the local concentration is introduced by considering adsorption equilibria on the surface, which precede the scale formation. For simplicity, the adsorption equilibria are assumed to be the same on the scale-covered and uncovered fractions of the surface.

To derive a mathematical model that represents the effects of scale formation on corrosion rates, we consider *n* separate species that may be formed on the surface of the corroding metal. The fraction of the surface occupied by *i*-th species is denoted by q_i. The change of the coverage fraction q_i with time, at a constant potential and for fixed activities of solution species, can be expressed as:

$$\left(\frac{\partial q_i}{\partial t}\right)_{E,a} = j_i\left(1-\sum_{k=1}^{n} q_k\right) - l_i q_i \qquad \text{i = 1, …, n} \tag{24}$$

where j_i is the rate constant for the formation of the *i*-th species on the free surface of the metal and l_i is the rate constant for the dissolution of this species. The rate of dissolution is proportional to the fraction of the surface covered by the *i*-th species. Eq. (24) is a system of *n* ordinary differential equations. This system may be solved for the coverage fractions q_i. In the limit of stationary state (i.e., for t $\rightarrow \infty$), the solution is

$$q_i = \frac{j_i}{l_i\left(1+\sum_{k=1}^{n}\frac{j_k}{l_k}\right)} \tag{25}$$

It can be further assumed that the partial current densities are modified by the presence of the scales, which reduce the surface area that is available for electrochemical reactions, i.e.,

$$i' = i(1 - \sum_{k=1}^{n} q_k) = \frac{i}{1 + \sum_{k=1}^{n} \frac{j_k}{l_k}} \tag{26}$$

where i denotes any of the partial current densities. Eq. (26) is a simplification because it implicitly assumes that the electrochemical processes do not proceed on the fraction of the surface that is covered by the solid scales. In general, various processes may occur on the scale surfaces (e.g., the reduction of protons or water), although their rates are significantly different from the rates on metal surfaces. Thus, eq. (26) should be regarded as a formula that represents the averaged effect of surface scales and does not necessarily reflect the microscopic coverage of the surface.

In general, the rates of scale formation depend on the activities of species that promote the precipitation of the scales. This is equivalent to the dependence on local supersaturation on the surface. Thus, j_k can be rewritten as

$$j_k = j_k^* N_X^a N_Y^b \ldots \tag{27}$$

where N_X, N_Y, etc., are surface concentrations of appropriate active solution species and a, b, etc., are reaction orders. In general, there can be any number of the species X, Y, etc. Thus, eq. (26) becomes

$$i' = \frac{i}{1 + \sum_{k=1}^{n} \frac{j_k^* N_X^a N_Y^b \ldots}{l_k}} = \frac{i}{1 + \sum_{k=1}^{n} q_k N_X^a N_Y^b \ldots} \tag{28}$$

where the symbol q_k is introduced for simplicity. The surface concentrations of the active ions result from adsorption processes on both the covered and free surfaces. Assuming the Langmuir adsorption behavior, N_X can be expressed as

$$N_X = \frac{K_X a_X}{1 + \sum_r K_r a_r} \tag{29}$$

Thus, in addition to the bulk activity of species, the effect of scale formation is determined by two parameters, i.e., q_k and K_r. The parameter q_k is the ratio of the rate constants for the formation and dissolution of the scale whereas K_r characterizes the adsorption of the aqueous species that are responsible for scale formation.

In the case of a $FeCO_3$ scale, the HCO_3^- ion can be assumed to be the active species that participates in the scale formation because it is much more abundant than CO_3^{2-} in the pH region of $FeCO_3$ precipitation, i.e.,

$$Fe + 2HCO_3^- = FeCO_3 + H_2CO_3 + 2e^- \tag{30}$$

Thus, N_{HCO3} is substituted for the term $N_X^a N_Y^b$ in eq. (28). Since N_{HCO3} depends on the activity of HCO_3^- ions, it is a strong function of solution chemistry. For the $FeCO_3$ scale, the parameter q_k has been found to be temperature-dependent according to an Arrhenius-type expression, i.e.,

$$q(T) = q(T_{ref}) \exp\left[-\frac{\Delta q}{R}\left(\frac{1}{T} - \frac{1}{T_{ref}} \right) \right] \tag{31}$$

Thus, the parameters that are needed for the computation of the effect of $FeCO_3$ scaling are $q_{FeCO3}(T_{ref})$, Δq_{FeCO3} and K_{HCO3}.

It should be noted that the thermodynamic stability of a solid phase such as $FeCO_3$ or FeS is insufficient for the formation of a protective scale. For example, formation of $FeCO_3$ on corroding surfaces has been observed under conditions that are not conducive to the reduction in corrosion rates.[37,40] $FeCO_3$ scales become protective at elevated temperatures whereas the precipitation of a nonprotective $FeCO_3$ phase may be observed at relatively low temperatures. From the point of view of the model, the protectiveness of the scale is primarily determined by the ratio of the reaction rate constants for the formation and dissolution of the scale on the surface of the metal. At the same time, the thermodynamic stability of the scale-forming solid depends on its solubility product, which is unrelated to the surface. These two properties may or may not coincide at given conditions.

Effect of H_2S

Hydrogen sulfide is known to form iron sulfide scales with different crystalline structures, which may or may not be protective depending on conditions such as temperature, pH or H_2S concentration.[17,18,20,23,24] In addition, H_2S contributes to the cathodic and anodic processes by modifying their mechanisms.[20,21] The effect of scale formation can be reproduced by using eqs. (28) and (29). For this purpose, the HS^- ions are considered to be the primary surface species that participate in the formation of FeS scales, i.e.,

$$Fe + 2HS^- = FeS + H_2S + 2e^- \tag{32}$$

If both $FeCO_3$ and FeS can be formed, eq. (28) becomes:

$$i' = \frac{i}{1 + q_{FeCO_3} N_{HCO_3^-} + q_{FeS} N_{HS^-}} \tag{33}$$

where the surface concentrations of HCO_3^- and HS^- are calculated from eq. (29). Eq. (33) is an approximation because it does not recognize the existence of various crystalline forms of FeS. However, it is appropriate for a preliminary analysis.

When sufficient concentration of hydrogen sulfide is available in the solution, H_2S contributes to the cathodic hydrogen discharge by the overall reaction

$$H_2S_{aq} + 2e^- = H_2 + 2HS^- \tag{34}$$

Morris et al.[21] found that a limiting current density in an acidic solution gradually disappears as the concentration of H_2S is increased. At the same time, the Tafel slope remains practically unchanged. This provides a strong indication that reaction (34) proceeds entirely under activation control and is not limited by the diffusion of H_2S to the surface. Therefore, we can tentatively propose the following expression for the partial current density for H_2S reduction:

$$i_{H_2S} = i^0_{H_2S} \exp\left[\frac{-a_{H_2S} F\left(E - E^0_H\right)}{RT}\right] \tag{35}$$

where the transfer coefficient is identical to that for proton reduction and the exchange current density is proportional to the activity of dissolved H_2S, i.e.,

$$i^0_{H_2S} = i^*_{H_2S} a_{H_2S} a^{2.2}_{H_2O} \tag{36}$$

where we retain the dependence on water activity that was determined for proton and water reduction.

In addition to the cathodic reaction, the presence of H_2S affects the anodic iron dissolution. Shoesmith et al.[20], following an earlier work by Iofa et al.[22], proposed that HS^- ions adsorb on the surface of the metal and, subsequently, accelerate the anodic dissolution of iron:

$$Fe + H_2S \rightarrow FeSH^-_{ads} + H^+ \tag{37}$$

$$FeSH^-_{ads} \rightarrow FeSH^+_{ads} + 2e^- \tag{38}$$

Reactions (37) and (38) are followed by the hydrolysis of the adsorbed $FeSH^+_{ads}$ species. Shoesmith et al.[20] further observed that this mechanism is analogous to the usual, hydroxide-accelerated, mechanism of iron dissolution. Therefore, we propose to extend eq. (6) for the exchange current density of iron dissolution by including an additional term that is proportional to the surface coverage of HS^- ions instead of OH^- ions, i.e.,

$$i^0_{Fe} = i^*_{Fe} q_{OH} a^c_{H_2O} + i^*_{Fe}{}' q_{SH} a^c_{H_2O} \tag{39}$$

The validity of equations (36), (37) and (39) will be tested in this work using experimental data for H_2S and CO_2/H_2S corrosion.

Implementation of the model

The parameters of the electrochemical model have been determined by utilizing a large number of experimental polarization and corrosion rate data. To ensure the validity of the model under a substantial range of conditions, these data were not limited to CO_2/H_2S corrosion. In particular, the parameters for the proton reduction, water reduction and iron oxidation processes were determined from data on the corrosion of iron and mild steel in various mineral acids, bases and saline solutions.[35,38] CO_2 corrosion data were utilized only for establishing the parameters of the processes that are specific to CO_2 corrosion

(i.e., the reduction of carbonic acid and formation of a $FeCO_3$ scale). Similarly, H_2S corrosion data were used to compute parameters that are specific to H_2S corrosion. It is noteworthy that some elements of the model did not require any data fitting. In particular, the limiting current densities can be computed *a priori* for assumed flow conditions because the diffusivities of species and solution viscosity are calculated from independent models.[36,39]

The model described above has been implemented in a program for the prediction and analysis of corrosion rates. As input, the program accepts the composition of corrosive medium, temperature and pressure. Then, thermodynamic calculations are performed to compute the speciation of the system and predict the phases that are stable. Depending on the conditions, the system may be made up of an aqueous phase that includes electrolyte components, a gas phase, an organic-rich liquid and any number of solid phases. The thermodynamic calculations make it possible to obtain the concentrations and activities of individual species, which are used further as input for the electrochemical model. Additionally, the program returns the diffusivities of individual species and the viscosity of the aqueous phase.

To execute the electrochemical model, the program requires flow conditions as additional input. Currently, the flow conditions are limited to single-phase flow. In addition to static conditions, pipe flow, rotating disk or rotating cylinder conditions can be selected. Then, the program computes the current density – potential relationships for individual cathodic and anodic processes. Further, the individual processes are combined into a total predicted polarization curve. The corrosion potential is calculated by applying the mixed-potential theory, i.e.,

$$\sum i_{c,i} = \sum i_{a,j} \tag{40}$$

where $i_{c,i}$ and $i_{a,j}$ denote the i-th cathodic and j-th anodic process. Once the corrosion potential is obtained by solving eq. (40), the corrosion current density is also computed.

Once the calculations are complete, the program displays the predicted corrosion rates and current density – potential relationships. Also, the program makes it possible to perform parametric studies in which the effect of various variables (e.g., temperature, pressure, concentration of selected components, flow velocity, etc.) on corrosion rate can be analyzed.

Results and Discussion

The performance of the model was verified by comparing the calculated corrosion rates with experimental data that cover substantial ranges of temperature, pH and partial pressures of CO_2 and H_2S. First, calculations have been made for systems that are not likely to form protective scales. Figure 2 shows the results for carbon steel in a 1 % NaCl solution in the presence of CO_2 at 1 bar and various temperatures and pH values. Pipe flow conditions with a velocity of 2 m/s and pipe diameter of 1.5 cm were assumed. It is noteworthy that the corrosion rates at pH values of 5 and 6 are nearly identical whereas the rate at pH=4 is significantly higher. In all cases, the experimental data of Nesic et al.[12] are reproduced with good accuracy. Figures 3 and 4 show the predicted current density – potential relationship and partial cathodic and anodic processes that are responsible for the corrosion rates shown in Figure 2. Figure 3 shows that two cathodic processes are important at pH=4, i.e., the reduction of H^+ ions (denoted by the curved marked by "1" in Figure 3) and the reduction of H_2CO_3 (marked by "2").

The total cathodic curve is determined by a superposition of these two processes and the reduction of H_2O (marked by "3"). The location of the mixed potential is marked by "x". At pH=6, the H^+ reduction process (marked by "1" in Figure 4) becomes unimportant because of the low concentration of H^+ ions. This shifts the limiting current density for H^+ reduction to a low value in Figure 4. Thus, the reduction of H_2CO_3 remains as the only dominant cathodic process. In general, the significance of the H^+ reduction process significantly decreases for pH values above 4.

Figures 5 and 6 show the effect of total pressure on the corrosion rate of carbon steel at temperatures ranging from 15 to 80 °C. It has been shown by de Waard and Milliams[1] that the rate of CO_2 corrosion is proportional to the partial pressure of CO_2. The model predictions are consistent with this observation. As shown in Figure 5, the rate is a nearly linear function of total pressure at lower temperatures (i.e., 15 and 22 °C). At these temperatures, the total pressure is practically equal to the partial pressure of CO_2. At higher temperatures (i.e., 60 and 80 °C), the partial pressure of water becomes significant and the CO_2 partial pressure is no longer close to the total pressure. Therefore, the plots of corrosion rate against the total pressure show a significant curvature at higher temperatures even though the variation of rates with partial CO_2 pressure remains nearly linear. The data of de Waard and Milliams[1] for a 0.1 % NaCl solution and those of Ikeda et al.[37] for synthetic seawater are represented essentially within experimental uncertainty as shown in Figures 5 and 6, respectively.

Figure 7 shows the effect of temperature on the corrosion of carbon steel in synthetic seawater. In this case, the formation of a protective $FeCO_3$ scale is responsible for a rapid decrease in the corrosion rate above approximately 90 °C. This effect is accurately represented by the model. In general, the exact location of the corrosion rate maximum depends on the partial pressure of CO_2 and concentration of HCO_3^- ions.

After verifying the model for CO_2 corrosion, calculations have been performed for systems containing both CO_2 and H_2S. Figure 8 shows the results for Armco iron in a 400 ppm NaCl solution at 30 °C and total pressure of 1 atm. The partial pressure of H_2S was varied from approximately 10^{-6} to 0.5 atm. At 30 °C, no $FeCO_3$ scale is likely to form. Therefore, the only solid phase that forms in the system is iron sulfide. As shown in Figure 8, the scale is moderately protective and it reduces the corrosion rate by a factor of approximately four (cf. the plateau range in Figure 8). The FeS scale formation becomes noticeable at very low partial pressures of H_2S (ca. $2\cdot10^{-6}$ atm). The corrosion rate drops significantly for partial pressures ranging from $2\cdot10^{-6}$ to 10^{-4} atm and reaches a plateau in a relatively wide range of H_2S partial pressures above 10^{-4} atm. The model reproduces the data of Greco and Wright[17] with very good accuracy. Also, it is consistent with the more recent data of Videm and Kvarekval[53], who demonstrated that an H_2S partial pressure of $4.5\cdot10^{-4}$ atm leads to a reduction of corrosion rate that is similar to that shown in the plateau range in Figure 8. It should be noted that the results shown in Figure 8 have been obtained for a strictly deaerated, static solution containing a low concentrations of chloride ions. In typical systems encountered in the industry, several factors such as trace amounts of oxygen, increased concentrations of chlorides or flow turbulence may interfere with the formation of adherent FeS scales[54]. Because of these factors, the threshold H_2S partial pressure that is necessary for the reduction of corrosion rates may be higher than the amount shown in Figure 8. For example, a reduction in corrosion rates has been reported when the H_2S partial pressure exceeds 10^{-3} atm in some systems.

At substantial H_2S partial pressures (above ca. 10^{-2} atm), the aqueous H_2S_{aq} and HS^- species become sufficiently concentrated to manifest themselves in the cathodic and anodic processes (cf. eqs. 36 and 39). This is responsible for an increase in the corrosion rate as shown in Figure 8. At the H_2S partial pressure of 0.5 atm, the corrosion rate becomes higher than that in the absence of H_2S. Figures 9 and 10

demonstrate the partial processes that are responsible for this behavior. Figure 9 shows the predicted current density – potential relationships when the partial pressure of H_2S is 0.01 atm. In this case, the dominant cathodic process is the reduction of H_2CO_3 (marked by "3" in Figure 9). It should be noted that the model does not predict any passive behavior in the current density – potential relationship. The reduction in corrosion rate is due to a shift of both cathodic and anodic processes to lower current densities, which is caused by a partial coverage of the metal surface by FeS. The lack of passivity is in agreement with experimental polarization data for CO_2 + H_2S systems[40]. In Figure 9, the current density that corresponds to the reduction of H_2S (marked by "2") is small because of a small concentration of H_2S and does not contribute to the corrosion rate. On the other hand, Figure 10 shows that the current density for H_2S reduction becomes very substantial when the partial pressure of H_2S increases to 0.23. In this case, H_2S reduction is predicted to contribute more to the total cathodic current density than H_2CO_3 reduction. The anodic current density is also somewhat increased in agreement with eq. (39), although the effect of H_2S on the anodic process is less significant. It should be noted that the iron sulfide scale is predicted to remain at $P_{H2S}>10^{-2}$ atm. However, the scale no longer reduces the corrosion rate because of the effect of increased H_2S concentrations on active dissolution. The obtained variation of corrosion rate with H_2S partial pressure is in very good agreement with the experimental data of Greco and Wright[17] (cf. Figure 8).

Conclusions

A comprehensive model has been developed for the simulation of CO_2/H_2S corrosion of carbon steels. The model combines thermodynamic speciation calculations with electrochemical computations based on the mixed-potential theory. The electrochemical model takes into account various partial cathodic and anodic processes, which may be under activation or mass transfer control. It includes the effects of protective scales such as iron carbonate or iron sulfide. The model has been verified by comparing calculated corrosion rates with experimental data over substantial ranges of temperature, pH and partial pressures of CO_2 and H_2S. Very good agreement with the data has been obtained.

The model has been incorporated into a computer program that is convenient for studying the effects of changing conditions such as temperature, pressure, stream composition or flow velocity on general corrosion rates. Since the model is based on a comprehensive speciation of aqueous systems and a mechanistic approach to electrochemical kinetics, it can be readily extended to systems with more complex chemistry and/or more complex flow conditions.

References

1. C. de Waard, D. E. Milliams, Corrosion, v. 31, p. 177-181 (1975).
2. C. de Waard, U. Lotz, D. E. Milliams, Corrosion, v. 47, p. 976 (1991).
3. S. Kanwar, W. P. Jepson, CORROSION/94, paper no. 24, NACE International, Houston, TX (1994).
4. R. Zhang, M. Gopal, W. P. Jepson, CORROSION/97, paper no. 601, NACE International, Houston, TX (1997).
5. L. K. Gatzky, R. H. Hausler, "A Novel Correlation of Tubing Corrosion Rates and Gas Production Rates", *in* R.H. Hausler, H. P. Godard, Advances in CO_2 Corrosion, Vol. 1, p. 87,

NACE International, Houston, TX (1984).
6. J.-L. Crolet, M. R. Bonis, "A Tentative Method for Predicting the Corrosivity of Wells in New CO_2 Fields", in P. A. Burke, A. I. Asphahani, B. S. Wright, Advances in CO_2 Corrosion, Vol. 2, p. 23, NACE International, Houston, TX (1985).
7. M. R. Bonis, J.-L. Crolet, CORROSION/89, paper no. 466, NACE International, Houston, TX (1989).
8. R. H. Hausler, J. D. Garber, CORROSION/90, paper no. 45, NACE International, Houston, TX (1990).
9. J. D. Garber, F. H. Walters, R. R. Alapati, C. D. Adams, CORROSION/94, paper no. 25, NACE International, Houston, TX (1994).
10. S. Kanwar, W. P. Jepson, CORROSION/94, paper no. 24, NACE International, Houston, TX (1994).
11. R. Zhang, M. Gopal, W. P. Jepson, CORROSION/97, paper no. 601, NACE International, Houston, TX (1997).
12. S. Nesic, J. Postlethwaite, S. Olsen, Corrosion, v. 52, p. 280-294 (1996).
13. S. Srinivasan, R. D. Kane, CORROSION/96, paper no. 11, NACE International, Houston, TX (1996).
14. A. Dugstad, L. Lunde, K. Videm, CORROSION/94, paper no. 14, NACE International, Houston, TX (1994).
15. L. G. S. Gray, B. G. Anderson, M. J. Danysh, P. R. Tremaine, CORROSION/90, paper no. 40, NACE International, Houston, TX (1989).
16. E. Dayalan, F. D. de Moraes, J. R. Shadley, S. A. Shirazi, E. F. Rybicki, CORROSION/98, paper no. 51, NACE International, Houston, TX (1989).
17. E. C. Greco, W. B. Wright, Corrosion, v. 18, p. 119t-124t (1962).
18. J. B. Sardisco, W. B. Wright, E. C. Greco, Corrosion, v. 19, p. 354t (1963).
19. K. Videm, J. Kvarekval, Corrosion, v. 51, p. 260-269 (1995).
20. D. W. Shoesmith, P. Taylor, M. G. Bailey, D. Owen, J. Electrochem. Soc., v. 127, p. 1007-1015 (1980).
21. D. R. Morris, L. P. Sampaleanu, D. N. Veysey, J. Electrochem. Soc., v. 127, p. 1228-1235 (1980).
22. Z. A. Iofa, V. V. Batrakov, Cho-Ngok-Ba, Electrochim. Acta, v. 9, p. 1645 (1964).
23. D. W. Shoesmith, P. Taylor, M. G. Bailey, B. Ikeda, Electrochim. Acta, v. 23, p. 903-916 (1978).
24. D. W. Shoesmith, M. G. Bailey, B. Ikeda, Electrochim. Acta, v. 23, p. 1329-1339 (1978).
25. J.F. Zemaitis, Jr., D. M. Clark, M. Rafal, N. C. Scrivner, Handbook of aqueous electrolyte thermodynamics: AIChE, New York, NY, 852 p. (1986).
26. M. Rafal, J. W. Berthold, N. C. Scrivner, S. L. Grise, Models for electrolyte solutions, *in* S. I. Sandler, ed., Models for Thermodynamic and Phase Equilibria Calculations: M. Dekker, New York, NY, p. 601-670 (1995).
27. A. Anderko, P. J. Shuler, CORROSION/98, paper no. 64: NACE International, Houston, TX (1998).
28. D. M. Drazic, Iron and Its Electrochemistry in an Active State, *in* B. E. Conway, J. O'M. Bockris, R. E. White, eds., Modern Aspects of Electrochemistry, No. 19 : Plenum Press, New York, NY, p. 69-192.
29. J. O'M. Bockris, D. Drazic, A. R. Despic, Electrochim. Acta, v. 4, p. 325-361 (1961).
30. E. J. Kelly, J. Electrochem. Soc., v. 112, p. 124-131 (1965).
31. N. G. Smart and J. O'M. Bockris, Corrosion, v. 48, p. 277-280 (1992).
32. K. J. Vetter, Electrochemical Kinetics: Academic Press, New York, NY (1967).

33. J. M. West, Electrodeposition and Corrosion Processes: Van Nostrand, New York, NY (1964).
34. A. Wieckowski, E. Ghali, M. Szklarczyk, J. Sobkowski, Electrochim. Acta, v. 28, p. 1619-1626 (1983).
35. B. D. Craig, D. S. Anderson, eds., Handbook of Corrosion Data: ASM International, Materials Park, OH (1995).
36. A. Anderko, M. M. Lencka, Ind. Eng. Chem. Res., v. 37, p. 2878-2888 (1998).
37. A. Ikeda, M. Ueda, S. Mukai, *in* R. H. Hausler and H. P. Godard, eds., Advances in CO_2 Corrosion, Vol. 1: NACE, Houston, TX, p. 39-51 (1984).
38. P. B. Mathur, T. Vasudevan, Corrosion, v. 38, p. 171-178 (1982).
39. M. M. Lencka, A. Anderko, S.J. Sanders, R. D. Young, Int. J. Thermophysics, v. 19, p. 367-378 (1998).
40. N. Sridhar, D.S. Dunn, A. Anderko, M.M. Lencka, Final Report PR-15-9712, Pipeline Research Committtee International, Arlington, VA (1998).
41. H. C. Helgeson, D. H. Kirkham, G. C. Flowers, Am. J. Sci., v. 281, p. 1249-1516 (1981).
42. J. C. Tanger, H. C. Helgeson, Am. J. Sci., v. 288, p. 19-98 (1988).
43. E. L. Shock, H. C. Helgeson, Geochim. Cosmochim. Acta, v. 52, p. 2009-2036 (1988).
44. E. L. Shock, H. C. Helgeson, Geochim. Cosmochim. Acta, v. 54, p. 915-943 (1990).
45. D. A. Sverjensky, Reviews in Mineralogy, v. 17, p. 177-209 (1987).
46. L. A. Bromley, AIChE J., v. 19, p. 313-320 (1973).
47. K. S. Pitzer, J. Phys. Chem., v. 77, p. 268-277 (1973).
48. G. Soave, Chem. Eng. Sci., v. 27, p. 1197-1203 (1972).
49. H. P. Meissner, *in* S.A. Newman, ed., Thermodynamics of Aqueous Systems with Industrial Applications: Am. Chem. Soc. Symp. Ser., v. 133, p. 495-511 (1980).
50. V.G. Levich, Physicochemical Hydrodynamics: Prentice-Hall, Englewood Cliffs, NJ, 700 p. (1962).
51. F. P. Berger, K.-F. F. L. Hau, Int. J. Heat Mass Trans., v. 20, p. 1185-1194 (1977).
52. M. Eisenberg, C. W. Tobias, C. R. Wilke, J. Electrochem. Soc., v. 101, p. 306-319 (1954).
53. K. Videm, J. Kvarekval, Corrosion, v. 51, p. 260-269 (1995).
54. F.F. Lyle, CO_2/H_2S Corrosion Under Wet Low-Flow Gas Pipeline Conditions in the Presence of Bicarbonate, Chloride and Oxygen, Final Report PR-15-9313: PRCI, American Gas Association, Arlington, VA (1997).

APPENDIX A

Thermodynamic Framework

In a multicomponent system, the partial molal Gibbs energy of the i-th species is related to the molality (m_i) by

$$\overline{G}_i = \overline{G}_i^{\,0} + RT \ln m_i g_i \qquad \text{(A-1)}$$

where $\overline{G}_i^{\,0}$ is the standard-state partial Gibbs energy and γ_i is the activity coefficient. Thus, the thermodynamic properties of the system can be calculated if the standard-state Gibbs energies are available for all species as functions of temperature and pressure (i.e., $\overline{G}_i^{\,0}(T,P)$) and the activity coefficients are known as functions of the composition vector **m** and temperature (i.e., $\gamma_i(\mathbf{m},T)$). From basic thermodynamics, the standard-state Gibbs energy of formation $\overline{G}_i^{\,0}(T,P)$ can be calculated as a function of temperature and pressure if the following data are available:

(1) Gibbs energy of formation at a reference temperature and pressure (usually, T_r = 298.15 K and P_r = 1 bar);
(2) Enthalpy of formation at T_r and P_r;
(3) Entropy at T_r and P_r;
(4) Heat capacity as a function of temperature and pressure and
(5) Volume as a function of temperature and pressure

The key to representing the standard-state properties over substantial temperature and pressure ranges is the accurate knowledge of the heat capacity and volume. For this purpose, the Helgeson-Kirkham-Flowers-Tanger[41-42] equation of state is used. This equation accurately represents the standard-state thermodynamic functions for aqueous, ionic or neutral, species as functions of both temperature and pressure. In its revised form[42], the HKF equation is capable of reproducing the standard-state properties up to 1000 °C and 5 kbar.

The HKFT equation is based on the solvation theory and expresses the standard-state thermodynamic functions as sums of structural and solvation contributions, the latter being dependent on the properties of the solvent (i.e., water). The standard partial molal volume ($\overline{V}^{\,0}$) and heat capacity ($\overline{C}_p^{\,0}$) are given by:

$$\overline{V}_0 = a_1 + \frac{a_2}{\Psi + P} + \left(a_3 + \frac{a_4}{\Psi + P} \right) \left(\frac{1}{T - \Theta} \right) - \omega\, Q + \left(\frac{1}{\varepsilon} - 1 \right) \left(\frac{\partial \omega}{\partial P} \right)_T \qquad \text{(A-2)}$$

$$\overline{C}_p^{\,0} = c_1 + \frac{c_2}{(T-\Theta)^2} - \left(\frac{2T}{(T-\Theta)^3} \right) \left(a_3 (P - P_r) + a_4 \ln \frac{\Psi + P}{\Psi + P_r} \right) + \omega\, TX + 2TY \left(\frac{\partial \omega}{\partial T} \right)_P - T \left(\frac{1}{\varepsilon} - 1 \right) \left(\frac{\partial^2 \omega}{\partial T^2} \right)_P \qquad \text{(A-3)}$$

where a_1, a_2, a_3, a_4, c_1 and c_2 represent species-dependent nonsolvation parameters, T_r is the reference temperature of 298.15 K, P_r is the reference pressure of 1 bar, Ψ and Θ refer to solvent parameters equal to 2600 bars and 228 K, respectively, Q, X, and Y denote the Born functions given by

$$Q = \frac{1}{e}\left(\frac{\partial \ln e}{\partial P}\right)_T \tag{A-4}$$

$$X = \frac{1}{e}\left[\left(\frac{\partial^2 \ln e}{\partial T^2}\right)_P - \left(\frac{\partial \ln e}{\partial T}\right)_P^2\right] \tag{A-5}$$

$$Y = \frac{1}{e}\left(\frac{\partial \ln e}{\partial T}\right)_P \tag{A-6}$$

where ε is the dielectric constant of water and ω stands for the Born coefficient, which is defined for the j-th aqueous species by

$$\omega_j \equiv \omega_j^{abs} - Z_j \omega_{H^+}^{abs} \tag{A-7}$$

In equation (A-7), Z_j is the charge on the j-th aqueous species, $\omega_{H^+}^{abs}$ refers to the absolute Born coefficient of the hydrogen ion and ω_j^{abs} designates the absolute Born coefficient of the j-th species given by

$$\omega_j^{abs} = \frac{N^0 e^2 Z_j^2}{2 r_{e,j}} \tag{A-8}$$

where N^0 is the Avogadro number, e is the electron charge and $r_{e,j}$ denotes the effective electrostatic radius of the j-th species, which is related to the crystallographic radius $r_{x,j}$ by

$$r_{e,j} = r_{x,j} + |z_j|(k_z + g) \tag{A-9}$$

where k_z represents a charge-dependent constant equal to 0.0 for anions and 0.94 for cations and g denotes a generalized function of temperature and density. Thus, the HKF equation expresses the heat capacity and volume as functions of pure water properties and seven empirical parameters, which have been tabulated for large numbers of ions, complexes and neutral, both inorganic and organic, molecules. The remaining thermodynamic properties are obtained by thermodynamic integration using the values of the Gibbs energy, enthalpy and entropy at reference temperature and pressure as integration constants.

If the HKFT equation parameters are not available from the regression of experimental data, they can be estimated. For this purpose, Shock and Helgeson[43,44] presented correlations for most solution species except for complexes. Sverjensky[45] developed an estimation method for several classes of complexes. In addition to the HKF equation parameters, these methods make it possible to predict the reference-state enthalpy and entropy if the reference-state Gibbs energy is known. These and other estimation techniques have been reviewed in detail by Rafal et al.[26]

The activity coefficient model used for representing the solution nonideality is an extended form of an expression developed by Bromley.[46] The Bromley equation is a combination of the Debye-Hückel term for long-range electrostatic interactions and a semi-empirical expression for short-range interactions between cations and anions. In a multicomponent system, the activity coefficient of an ion i is given by

$$\log g_i = \frac{-Az_i^2 I^{1/2}}{1+I^{1/2}} + \sum_j^{NO}\left[\frac{|z_i|+|z_j|}{2}\right]^2\left[\frac{(0.06+0.6B_{ij})|z_i z_j|}{\left(1+\frac{1.5}{|z_i z_j|}I\right)^2} + B_{ij} + C_{ij}I + D_{ij}I^2\right]m_j \qquad \text{(A-10)}$$

where A is the Debye-Hückel coefficient which depends on temperature and solvent properties, z_i is the number of charges on ion i, I is the ionic strength (i.e., $I = 0.5\sum z_i^2 m_i$), NO is the number of ions with charges opposite to that of ion i, and B_{ij}, C_{ij} and D_{ij} are empirical, temperature-dependent cation-anion interaction parameters. Bromley's[46] original formulation contains only one interaction parameter, B_{ij}, which is sufficient for systems with moderate ionic strength. For concentrated systems, the two additional coefficients C_{ij} and D_{ij} usually become necessary. The three-parameter form of the Bromley model is capable of reproducing activity coefficients in solutions with ionic strength up to 30 mol/kg. The temperature dependence of the B_{ij}, C_{ij} and D_{ij} parameters is usually expressed using a simple quadratic function.

The Bromley model is restricted to interactions between cations and anions. For ion-molecule and molecule-molecule interactions, the well-known model of Pitzer[47] is used. To calculate the fugacities of components in the gas phase, the Redlich-Kwong-Soave[48] equation of state is used. In the absence of sufficient experimental data, reasonable predictions can be made using a method due to Meissner[49], which makes it possible to extrapolate the activity coefficients to higher ionic strengths based on only a single, experimental or predicted, data point.

APPENDIX B

Calculation of the Mass Transfer Coefficient

The mass transfer coefficient k_m (eq. 13) can be calculated once the flow geometry is assumed. For a rotating disk, the equation of Levich[50] holds:

$$k_m = 0.62 D^{2/3} \nu^{-1/6} \omega^{1/2} \qquad \text{(B-1)}$$

where D is the diffusion coefficient of the species that undergoes the electrode reaction, ν is the kinematic viscosity and ω is the rotation velocity. The diffusion coefficient and viscosity are calculated as functions of temperature and concentration using the methods developed by Anderko and Lencka[36] and Lencka et al.[39], respectively.

For straight pipe and rotating cylinder geometry, the mass transfer coefficient can be expressed in terms of the dimensionless Reynolds (Re) and Schmidt (Sc) numbers. These numbers are defined by:

$$Re = \frac{vd}{\nu} \qquad \text{(B-2)}$$

$$Sc = \frac{\nu}{D} \qquad \text{(B-3)}$$

where v is the linear velocity and d is the diameter. For single-phase flow in a straight pipe, the correlation of Berger and Hau[51] can be used, i.e.,

$$\frac{k_m d}{D} = 0.0165 Re^{0.86} Sc^{0.33} \qquad \text{(B-4)}$$

For a rotating cylinder, the correlation of Eisenberg et al.[52] applies, i.e.,

$$\frac{k_m d}{D} = 0.0791 Re^{0.70} Sc^{0.356} \qquad \text{(B-5)}$$

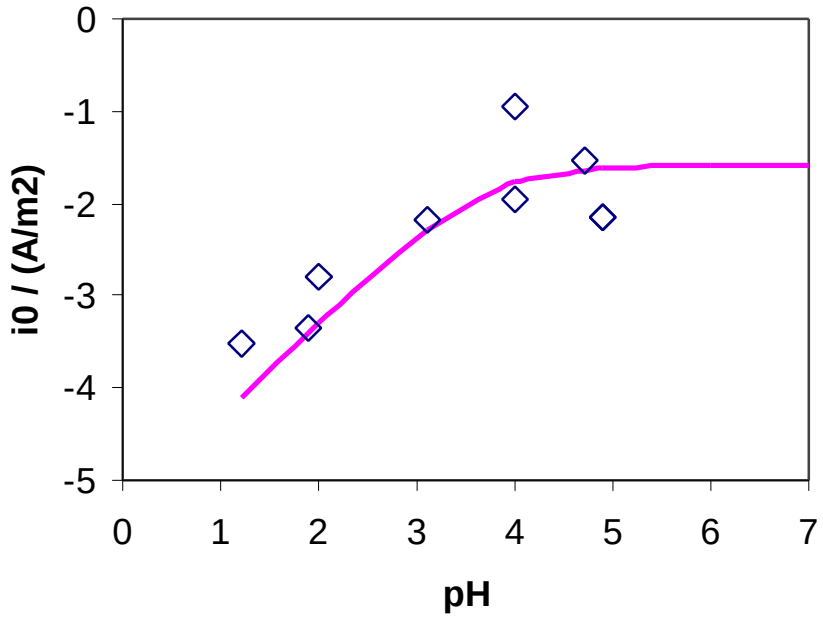

Figure 1. Representation of the exchange current density for iron dissolution at different pH values. The symbols denote the experimental data of Bockris et al.[29].

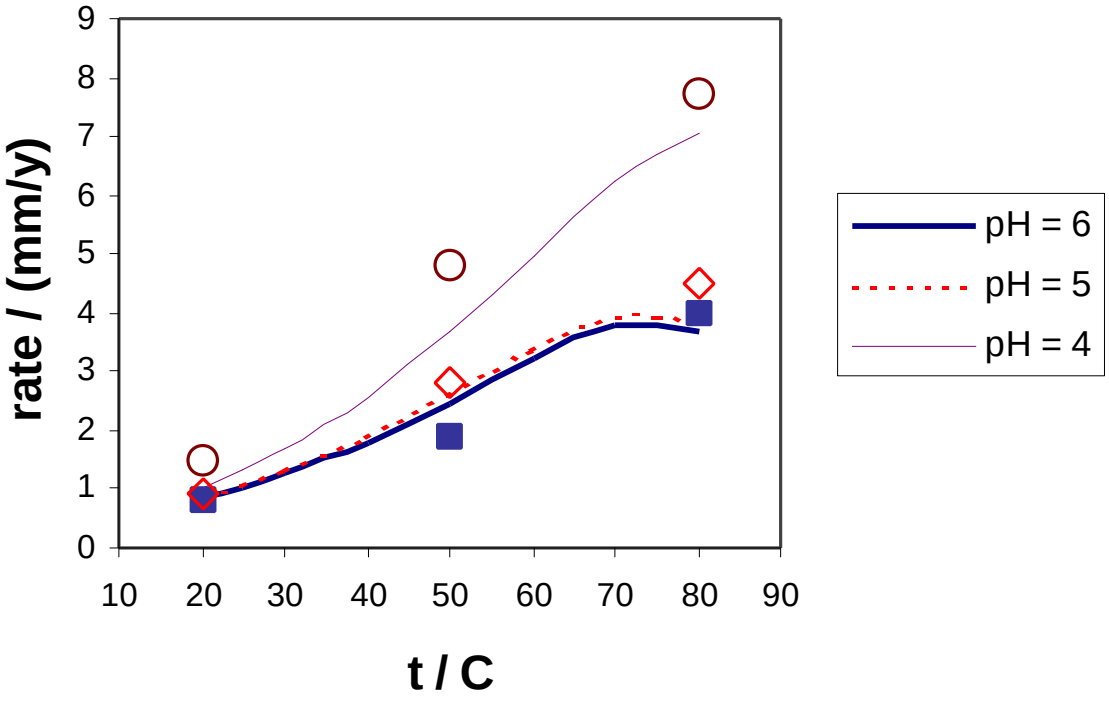

Figure 2. Corrosion rate for carbon steel in a 1 % NaCl solution in the presence of CO_2 at 1 bar under the conditions of pipe flow with a velocity of 2 m/s and pipe diameter of 1.5 cm. The lines have been obtained from the model and the symbols denote the data of Nesic et al.[12] for X-65 steel.

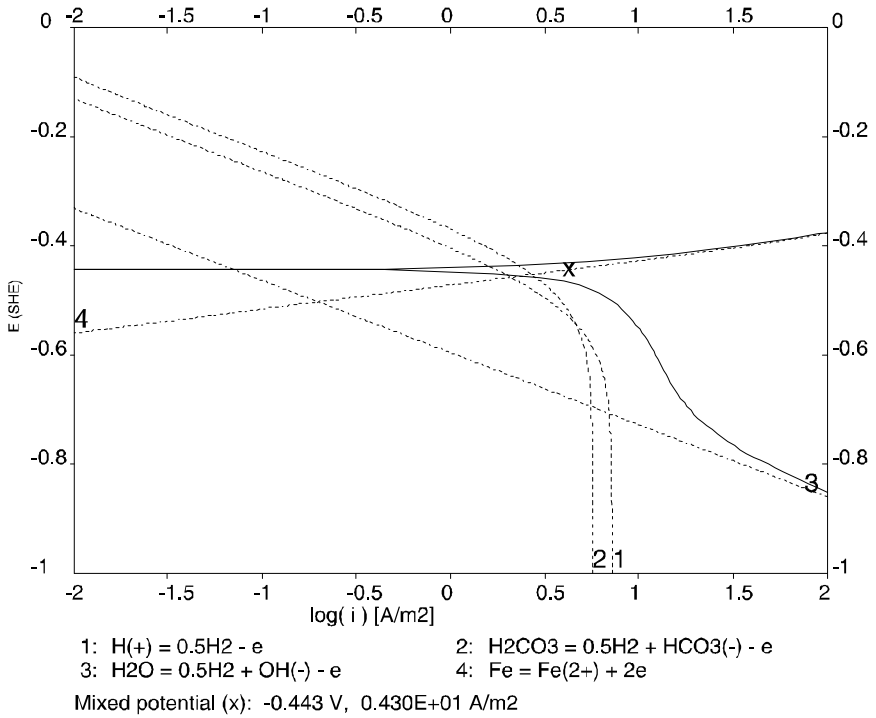

Figure 3. Predicted current density - potential relationship and partial cathodic and anodic processes for carbon steel in a 1 % NaCl solution in the presence of CO_2 at 1 bar and 60 °C under the conditions of pipe flow with a velocity of 2 m/s and pipe diameter of 1.5 cm. The natural pH of the system is 4.04.

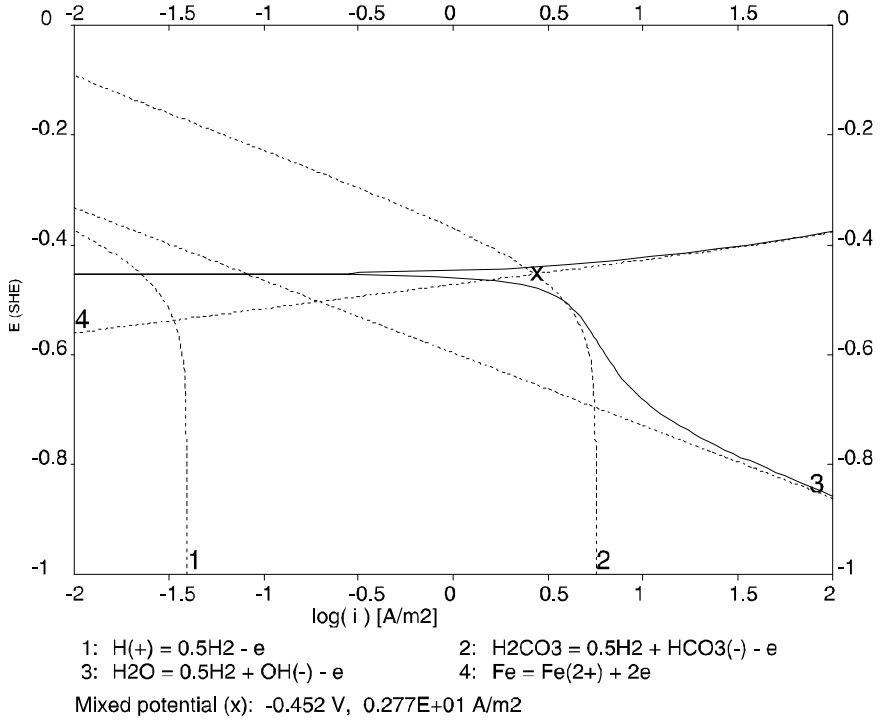

Figure 4. Predicted current density - potential relationship and partial cathodic and anodic processes for carbon steel in a 1 % NaCl solution in the presence of CO_2 at 1 bar and 60 °C under the conditions of pipe flow with a velocity of 2 m/s and pipe diameter of 1.5 cm. The pH of the system has been adjusted to 6 by adding NaOH.

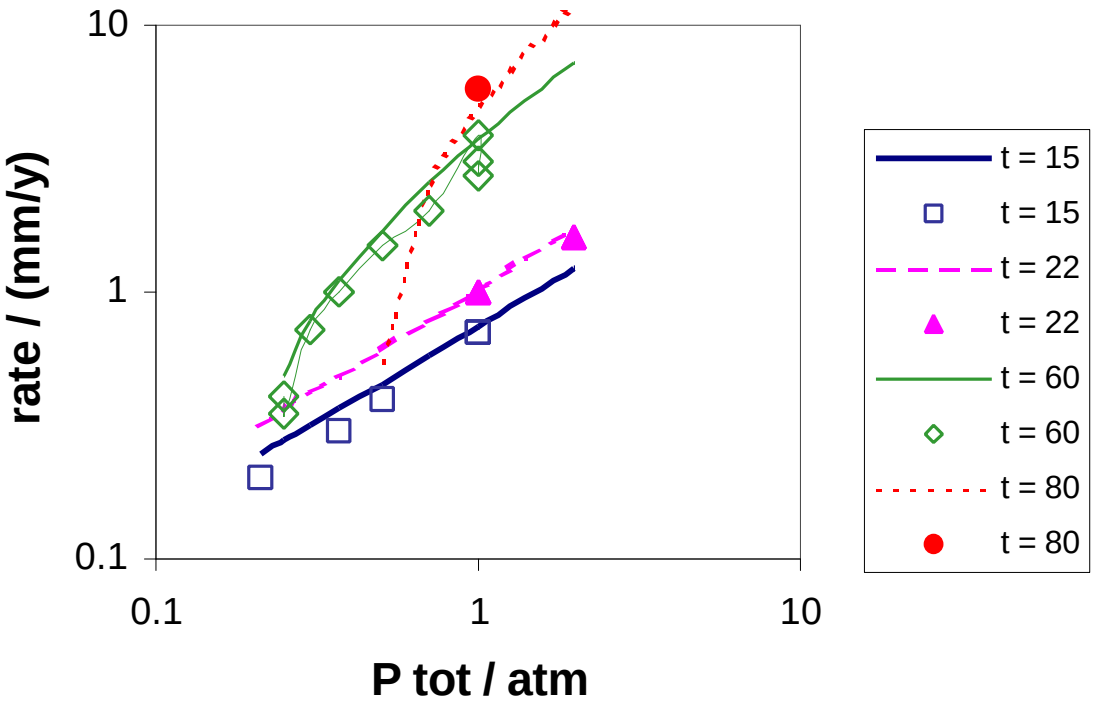

Figure 5. Corrosion rate as a function of total pressure for carbon steel in a 0.1 % NaCl solution in the presence of CO_2 at various temperatures. The lines have been obtained from the model and the symbols denote the data of de Waard and Milliams [1] for X-52 steel.

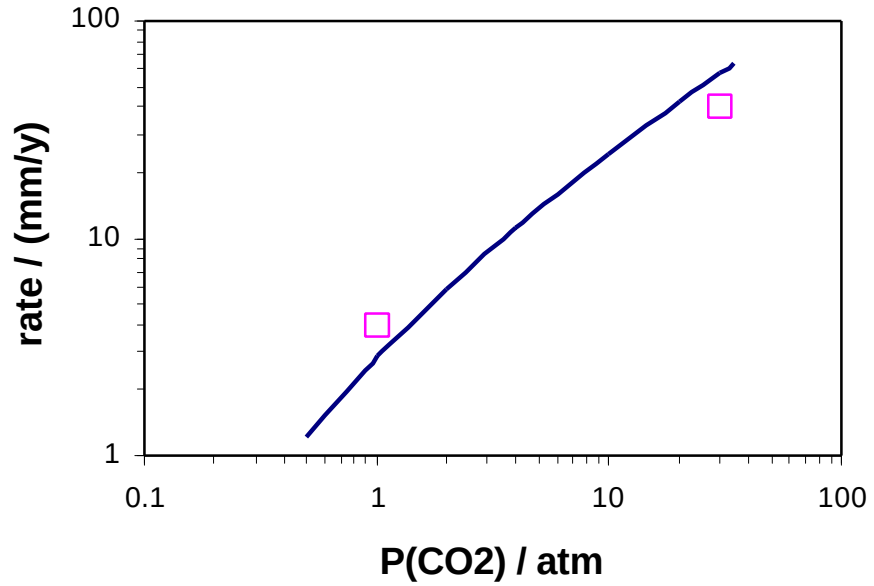

Figure 6. Corrosion rate as a function of pressure for carbon steel in synthetic seawater in the presence of CO_2 at 60 °C. The line has been obtained from the model and the symbols denote the data of Ikeda et al. [37]

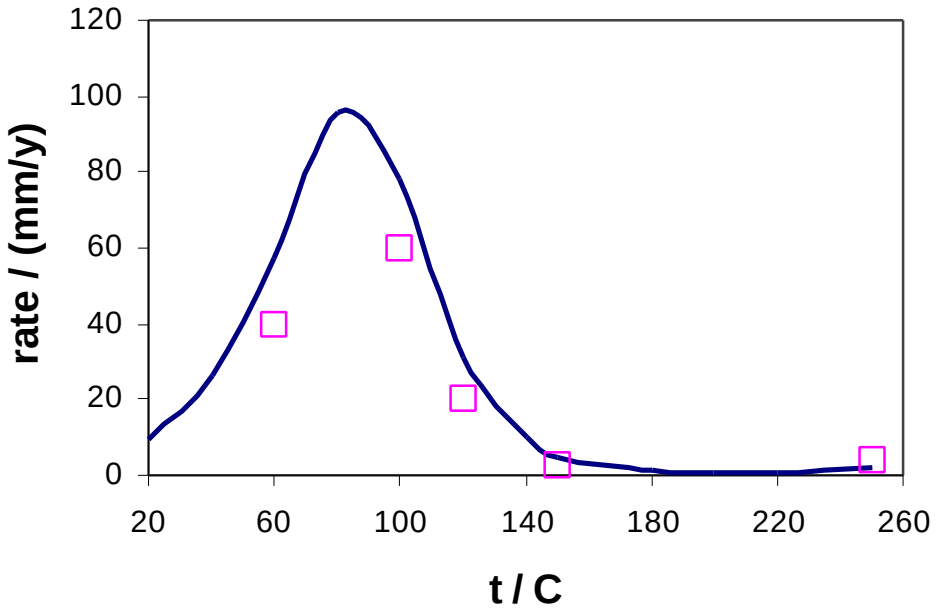

Figure 7. Corrosion rate as a function of temperature for carbon steel in synthetic seawater. The CO_2 pressure is 30 bar at room temperature. The line has been obtained from the model and the symbols denote the data of Ikeda et al.[37]

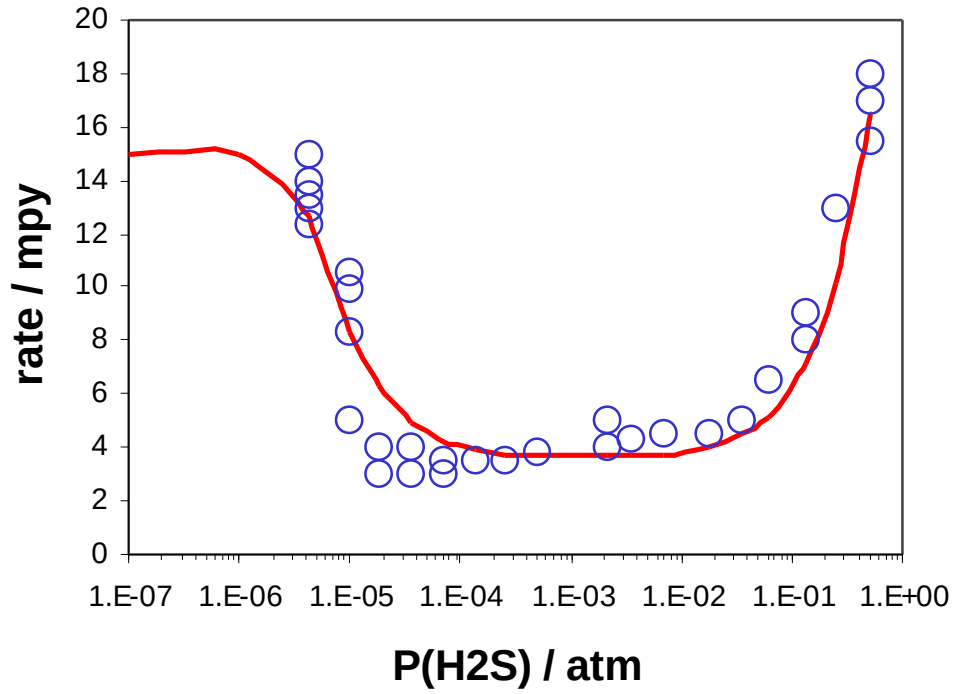

Figure 8. Corrosion rate as a function of H_2S partial pressure for Armco iron at 30°C. The total pressure (CO_2 and H_2S) is 1 atm. The line has been obtained from the model and the symbols denote the data of Greco and Wright.[17]

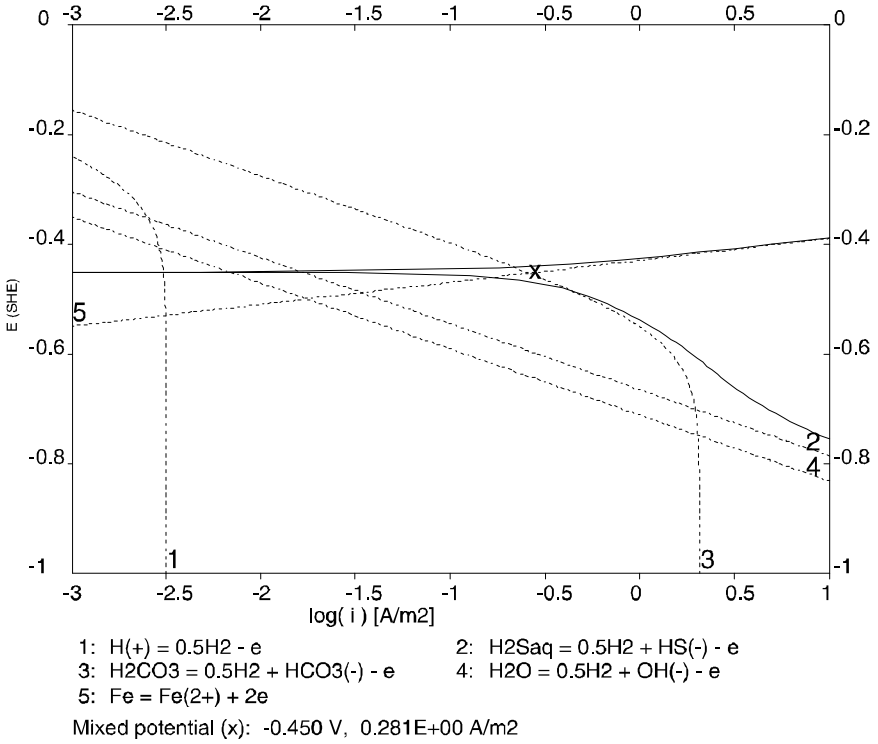

Figure 9. Predicted current density - potential relationship and partial cathodic and anodic processes for Fe in a CO_2+H_2S system at 30 °C under static conditions. The partial pressure of H_2S is 0.01 atm and the total pressure is 1 atm.

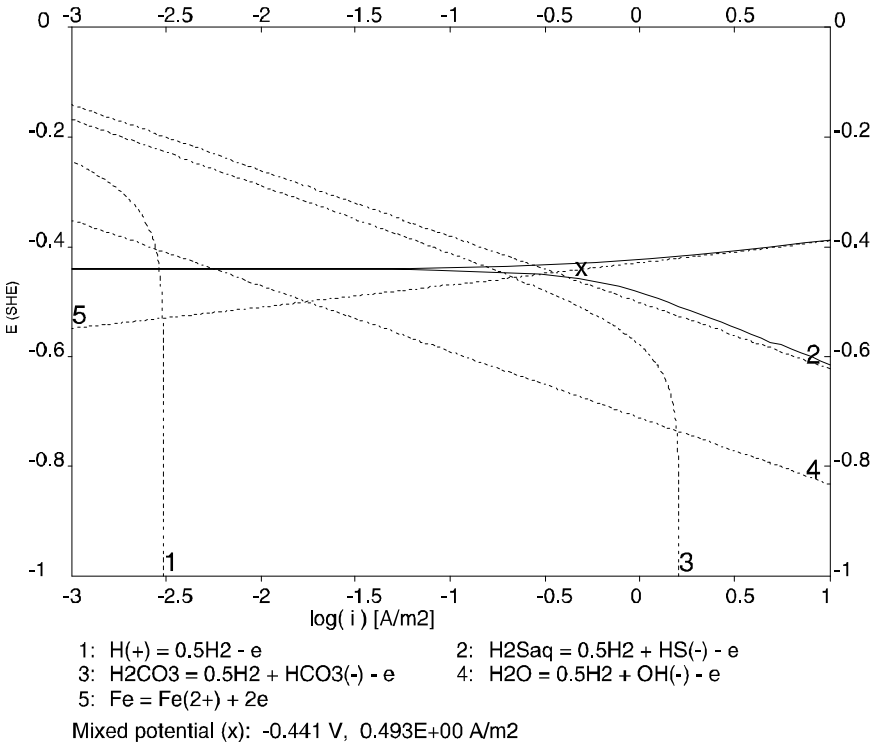

Figure 10. Predicted current density - potential relationship and partial cathodic and anodic processes for Fe in a CO_2+H_2S system at 30 °C under static conditions. The partial pressure of H_2S is 0.23 atm and the total pressure is 1 atm.